Development of high-vorticity structures in incompressible 3D Euler equations: comparison with exact solution.

D. Agafontsev [a], A. Mailybaev [b] and E. Kuznetsov [c].

[a] - *P.P. Shirshov Institute of Oceanology of RAS, Moscow, Russia.*

[b] - *Instituto Nacional de Matematica Pura e Aplicada - IMPA, Rio de Janeiro, Brazil.*

[d] - *P.N. Lebedev Physical Institute of RAS, Moscow, Russia.*

May 23d, 2017, Chernogolovka, Russia.

Abstract.

We integrate numerically the incompressible 3D Euler equations,

$$\frac{\partial \mathbf{v}}{\partial t} + (\mathbf{v}\cdot\nabla)\mathbf{v} = -\nabla p, \qquad \operatorname{div}\mathbf{v} = 0,$$

starting from generic large-scale initial conditions. We observe that a number of regions of high vorticity

$$\omega = \operatorname{rot}\mathbf{v},$$

develop with time, for each initial condition. Our main result is that, as we found, all of these regions are described with a novel exact solution of the 3D Euler equations. Contrary to the previously known solutions, our solution accurately reproduces the main characteristics of the high-vorticity regions.

For all initial conditions that we studied, there exists a universal Kolmogorov-type power law between the vorticity maximum and the pancake thickness,

$$\omega_{\max}(t) \sim \ell_1(t)^{-2/3}.$$

Some of the initial flows demonstrate with time emergence of the Kolmogorov-like energy spectrum $\mathbf{E_k \sim k^{-5/3}}$. The emergence of this spectrum can be influenced by specific choice of initial conditions.

1. Introduction.

We study numerically the incompressible 3D Euler equations,

$$\frac{\partial \mathbf{v}}{\partial t} + (\mathbf{v}\cdot\nabla)\mathbf{v} = -\nabla p, \qquad \operatorname{div}\mathbf{v} = 0.$$

- these are one of the most important equations in mathematical physics;
- the question of existence and uniqueness for their solutions at infinite time is yet to be discovered; the same question for the Navier-Stokes equations is one of the Millennium Prize Problems.

The question of existence and uniqueness is directly related to the problem of weather the Euler equations can develop a singularity in a finite time, i.e. collapse.

According to the Beale-Kato-Majda theorem, at the time of the collapse $\mathbf{t_0}$ (if it exists), the time integral of vorticity must explode,

$$\int_0^{t_0} \omega_{\max}(t)dt = +\infty,$$

so that the vorticity must turn to infinity too.

As was demonstrated by the early numerical studies, the vorticity maximum indeed tends to grow with time. If we start from generic initial conditions, this growth is exponential and the regions of high vorticity represent exponentially compressing pancake-like structures, see Brachet el al (1992).

1. Introduction.

Since the tendency toward a vortex sheet should suppress three-dimensionality of the flow, formation of a finite-time singularity is not expected; recall that the dynamics of the 2D Euler equations is known to be regular. Thus, further numerical studies were mainly concentrated on carefully designed initial conditions providing enhanced vorticity growth.

Despite the large effort we are still far from the reliable answer of whether the blow-up scenario is possible. And from the point of view of numerical simulations, there is no much hope that we will achieve this answer anytime soon.

This is why in our recent study D.S. Agafontsev, E.A. Kuznetsov, A.A. Mailybaev, *Development of high vorticity structures in incompressible 3D Euler equations*, Phys. Fluids 27, 085102 (2015), we decided to move in a different direction.

First, in the collapse studies, authors usually test carefully designed initial conditions. We decided to test rather generic initial flows.

Second, usually, only evolution of the global vorticity maximum is considered. We track down all the remaining local maximums as well. This allows us to examine other regions of high vorticity, test different distributions of local maximums, connect evolution of the high-vorticity structures with development of the energy spectrum.

1. Introduction.

We solve 3D Euler equations in the periodic box **[-π, π]³** in the vorticity formulation:

$$\frac{\partial \omega}{\partial t} = \mathrm{rot}\,[\mathbf{v} \times \omega], \quad \mathbf{v} = \mathrm{rot}^{-1}\omega.$$

Inverse rotor is uniquely defined under the conditions of zeroth average velocity and incompressibility,

$$\int \mathbf{v} d^3\mathbf{r} = 0, \qquad \mathrm{div}\,\mathbf{v} = 0,$$

and has a simple representation in Fourier space as

$$\mathbf{v} = \frac{i\mathbf{k} \times \omega}{k^2}.$$

We implement Runge-Kutta 4th order scheme combined with the cut-off function suggested by Hou & Li (2007) to deal with the bottle-neck instability,

$$\rho(\mathbf{k}) = \exp\left(-36\left[\left(k_1 / K_1\right)^{36} + \left(k_2 / K_2\right)^{36} + \left(k_3 / K_3\right)^{36}\right]\right).$$

We also performed comparison with the standard 2/3 dealiasing rule,

$$\rho(\mathbf{k}) = \begin{cases} 1 & \text{if} \quad |k_j| / K_j \le 2/3, \\ 0 & \text{if} \quad |k_j| / K_j > 2/3, \end{cases}$$

and found no difference in our results. Here $K_j = N_j / 2$ is the maximal wavenumber along j = x,y,z dimension.

1. Introduction.

We start from initial shear flow (exact solution),

$$\omega_x = \sin(z), \quad \omega_y = \cos(z), \quad \omega_z = 0,$$

plus periodic perturbation.

The simulations are started on **128^3** grid. At every time step we analyze the spectrum of our solution, and if we determine that the spectrum starts to excite near

$$(2/3)K_i = N_i/3,$$

we immediately increase the number of points in this particular direction. The solution from the old grid is transferred to the new grid with the help of Fourier interpolation which has error comparable to round-off for periodic boundary conditions.

The Fourier interpolation is based on the fact that the distance between the subsequent harmonics is fixed,

$$\Delta k = 2\pi / L = 1,$$

and the range of the spectrum depends on the number of points $\mathbf{N_j}$ along j-dimension as

$$k_i \in [-\pi/\Delta x_i, +\pi/\Delta x_i] = [-N_i/2, +N_i/2].$$

Therefore, we simply transfer the spectrum of our solution to the new Fourier space, and set all the newly added harmonics to zero.

1. Introduction.

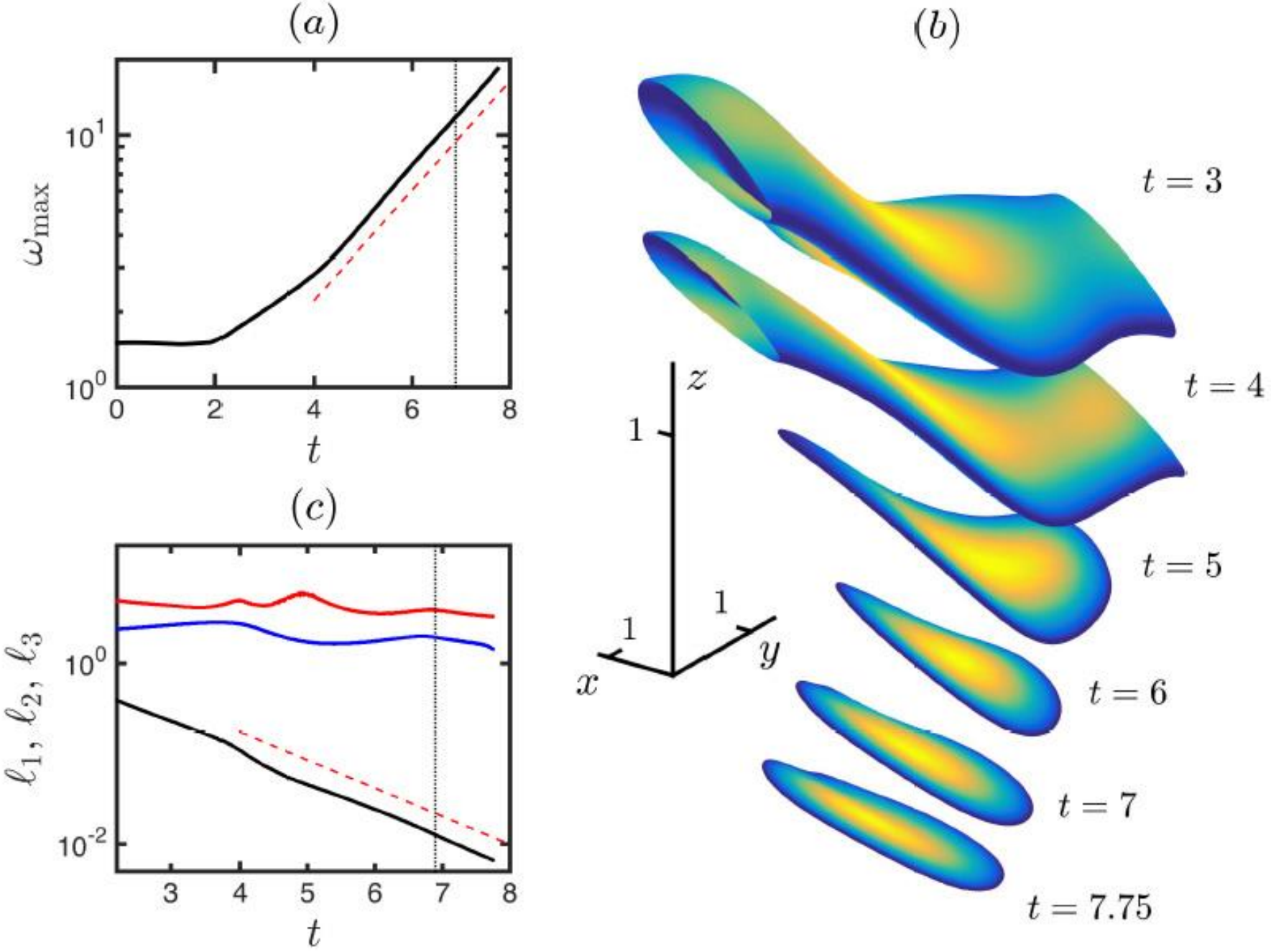

1. Introduction.

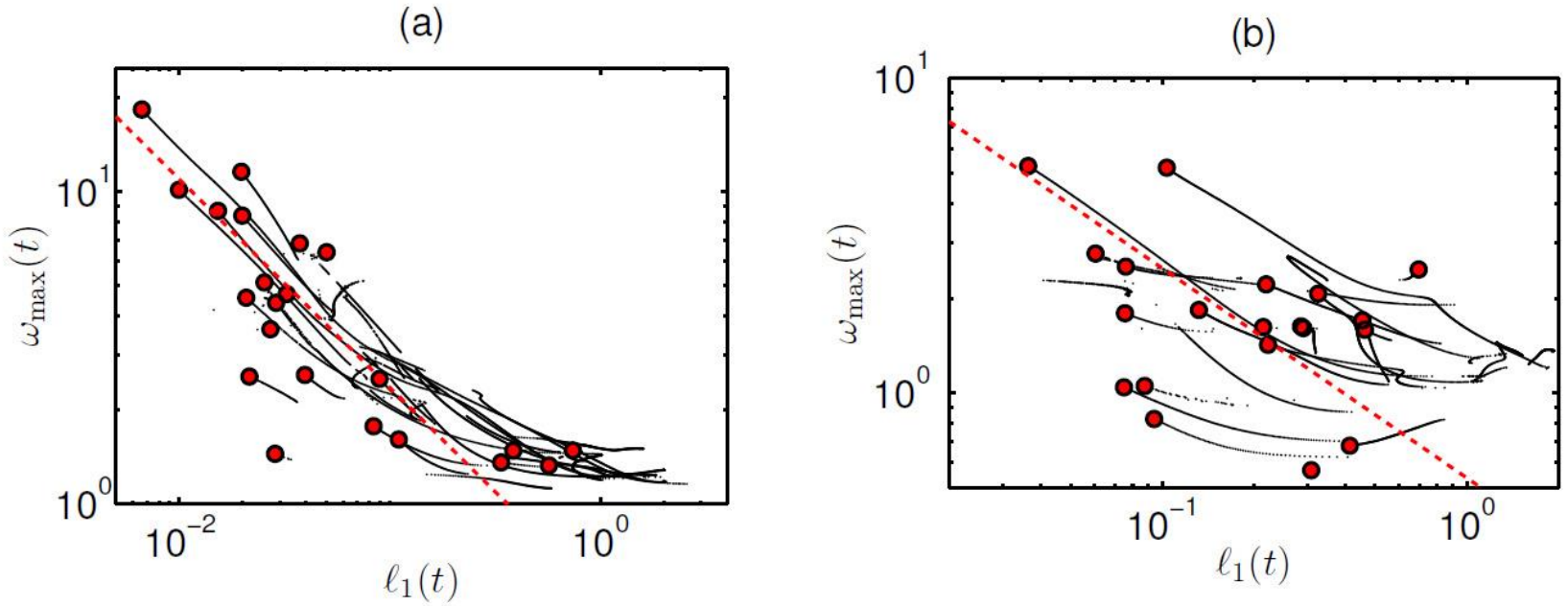

FIGURE 4. (a) Relation between the vorticity local maximums $\omega_{\max}(t)$ and the respective characteristic lengths $\ell_1(t)$ during the evolution of the pancake structures. Lines represent evolution of the maxima with increasing time, with the red dots corresponding to the final simulation time. The dashed red line indicates the power-law scaling $\omega_{\max} \propto \ell_1^{-2/3}$. (b) The same graph for a different simulation with a generic initial condition and the final grid $1152 \times 972 \times 864$.

During evolution of the pancake structures, there exists a Kolmogorov-type power-law between the vorticity maximum and the pancake thickness:

$$\omega_{\max}(t) \sim \ell_1(t)^{-2/3}.$$

1. Introduction.

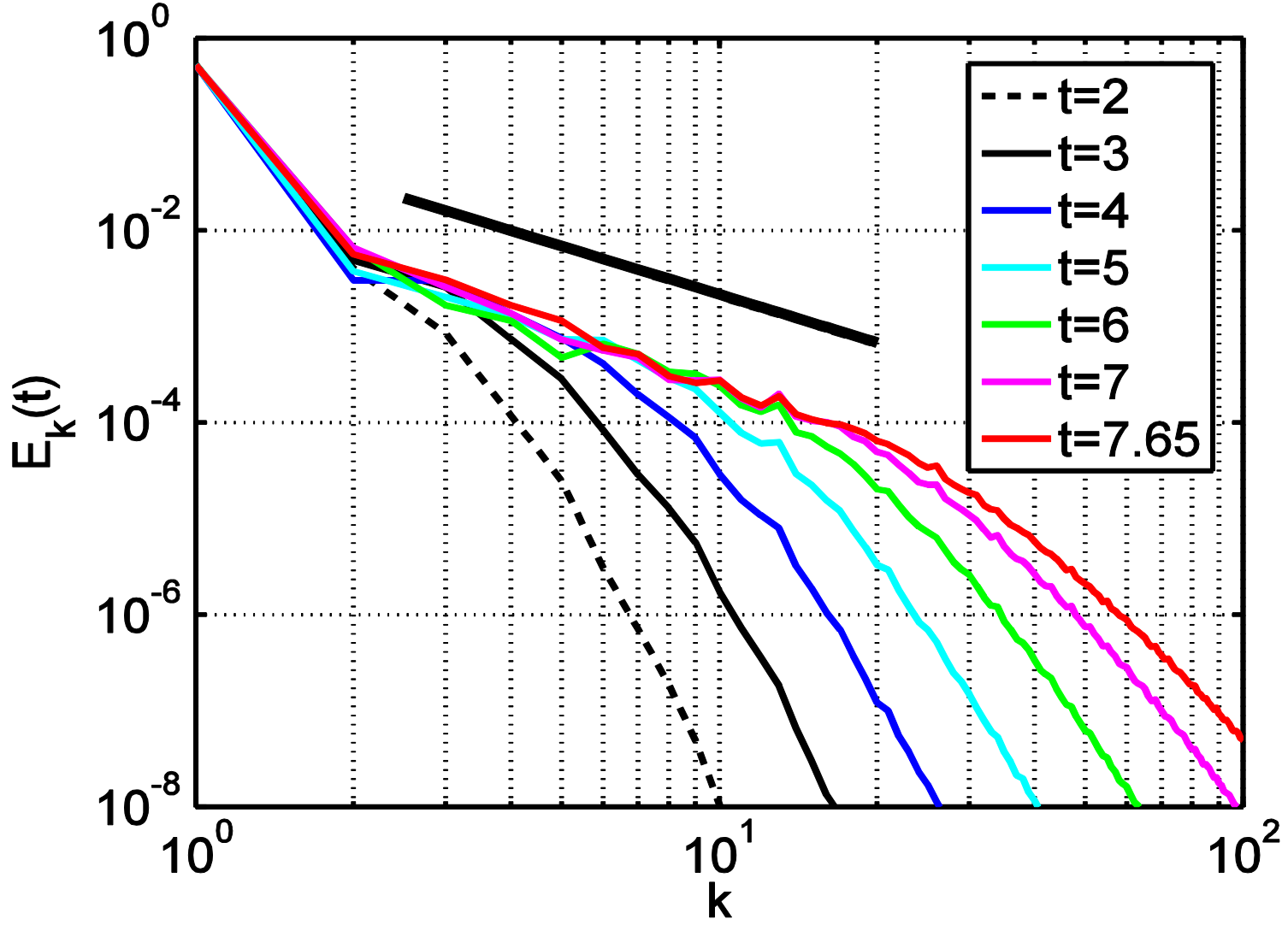

Tendency of the energy spectrum toward the Kolmogorov $\mathbf{k^{-5/3}}$ spectrum: for wavenumbers **2 ≤ k ≤ 30**, we observe

$$\varepsilon(k,t) \to const \times k^{-5/3}.$$

2. Exact solution of the Euler equations.

Following the numerical results, we suggest an analytical model for the vorticity growth. Assuming that in Cartesian coordinates **a** = a_1 $\mathbf{n_1}$ + a_2 $\mathbf{n_2}$ + a_3 $\mathbf{n_3}$ the vorticity changes only along $\mathbf{a_1}$-axis and is oriented along $\mathbf{a_2}$-axis, we write

$$\omega(\mathbf{a},t)=\omega_2\mathbf{n}_2,\quad \omega_2=\Omega(t)\,f'\left(\frac{a_1}{\ell_1(t)}\right).$$

where **Ω(t)** is the characteristic vorticity amplitude and $\mathbf{l_1(t)}$ is the pancake thickness. The ansatz contains a derivative (denoted by prime) of an arbitrary function **f(ξ)** taken at **ξ** = $\mathbf{a_1/l_1(t)}$. Together with the velocity field

$$\mathbf{v}(\mathbf{a},t)=-\Omega(t)\,\ell_1(t)\;f\left(\frac{a_1}{\ell_1(t)}\right)\mathbf{n}_3+\begin{pmatrix}-\beta_1(t)\,a_1\\ \beta_2(t)\,a_2\\ \beta_3(t)\,a_3\end{pmatrix},$$

this is exact solution of the 3D Euler equations (in the vorticity formulation)

$$\frac{\partial\omega}{\partial t}=\mathrm{rot}\,(\mathbf{v}\times\ \omega),\quad \mathbf{v}=\mathrm{rot}^{-1}\omega.$$

The functions $\beta_1(t)$, $\beta_2(t)$ and $\beta_3(t)$ are given by

$$\beta_1=-\dot{\ell}_1/\ell_1,\quad \beta_2=\dot{\Omega}/\Omega,\quad -\beta_1+\beta_2+\beta_3=0.$$

2. Exact solution of the Euler equations.

The velocity satisfies the Euler equations with the pressure

$$p = (\dot{\beta}_1 - \beta_1^2)\frac{a_1^2}{2} - (\dot{\beta}_2 + \beta_2^2)\frac{a_2^2}{2} - (\dot{\beta}_3 + \beta_3^2)\frac{a_3^2}{2}.$$

Main properties of the presented solution:

- It has infinite energy, so that in numerical simulations it can only be valid in a finite space;
- it allows for any time-dependency of vorticity **Ω(t)** and pancake thickness $\mathbf{l_1(t)}$, including the one leading to blowup;
- it shows that the Cauchy initial-value problem does not have unique solution if the energy is unlimited;
- it can be extended for the Navier-Stokes equations with kinematic viscocity **ν** if function **f(ξ,t)** changes with time as

$$f_t - \frac{\nu}{\ell_1^2} f_{\xi\xi} = 0.$$

2. Exact solution of the Euler equations.

The simplest form of the presented solution is when both the vorticity amplitude and pancake thickness behave exponentially like **$\Omega(t) \sim \exp(\beta_2 t)$** and **$l_1(t) \sim \exp(-\beta_1 t)$**. In this case they are connected with the power-law

$$\Omega(t) \propto \ell_1(t)^{-\zeta}, \quad \zeta = \beta_2 / \beta_1,$$

and the pressure does not explicitly depend on time.

The asymmetry of the straining flow is described with dimensionless parameter

$$\sigma = \frac{\beta_2 - \beta_3}{\beta_2 + \beta_3} = \frac{2\beta_2}{\beta_1} - 1, \quad \zeta = \frac{\sigma + 1}{2}.$$

The velocity jump at the scale of the pancake thickness vanishes with time for **$\sigma<1$** (**$\zeta<1$**), i.e. no Kelvin-Helmholtz instability for our case **$\sigma = 1/3$** and **$\zeta = 2/3$**:

$$\delta v_3 \propto \Omega \ell_1 \propto \ell_1^{1-\zeta}.$$

3. Comparison with numerical simulations.

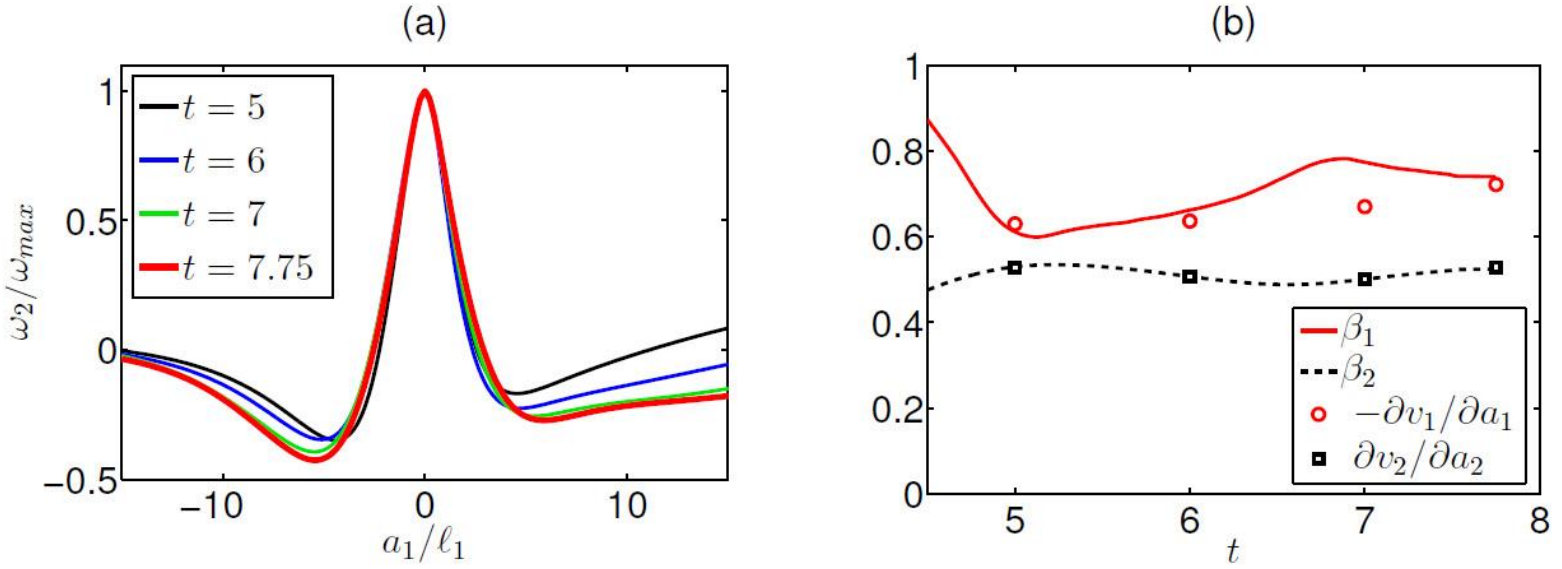

FIGURE 2. (a) Normalized vorticity component $\omega_2/\omega_{\max}$ as a function of $\xi = a_1/\ell_1$ at different times. (b) Comparison of the logarithmic derivatives $\beta_1 = -\dot{\ell}_1/\ell_1$ and $\beta_2 = \dot{\omega}_{\max}/\omega_{\max}$ with the velocity gradients $-\partial v_1/\partial a_1$ and $\partial v_2/\partial a_2$ computed at the global vorticity maximum, see Eq. (4.2). Prior computing the time derivatives, ℓ_1 and $\omega_{\max}$ are smoothed with the weighted local regression (lowess filter), see Cleveland *et al.* (1988).

The first test is related to self-similarity of the transversal vorticity profile, which should be kept as

$$\omega_2 / \omega_{\max} = f'(\xi), \quad \xi = a_1 / \ell_1.$$

Two relations should also be valid:

$$\partial v_1 / \partial a_1 = -\beta_1 = \dot{\ell}_1 / \ell_1, \qquad \partial v_2 / \partial a_2 = \beta_2 = \dot{\omega}_{\max} / \omega_{\max}.$$

3. Comparison with numerical simulations.

Checking the velocity field directly is difficult, since the solution can be modified by adding a uniform velocity field **(0,$v_{b2}(t)$,$v_{b3}(t)$)** with arbitrary time dependency. This is why we examine its gradients. According to the solution,

$$[\partial v_i / \partial a_j] = \begin{pmatrix} -\beta_1 & 0 & 0 \\ 0 & \beta_2 & 0 \\ -\omega_2 & 0 & \beta_3 \end{pmatrix}.$$

At the final time and at the global vorticity maximum we have

$$[\partial v_i / \partial a_j]_{\mathbf{a}=0} = \begin{pmatrix} -0.72 & -0.04 & -0.03 \\ -0.11 & 0.53 & -0.09 \\ -18.42 & -0.04 & 0.19 \end{pmatrix},$$

confirming the single large (3,1)-component $\partial v_3/\partial a_1 \approx -\omega_{max}$. The diagonal components are in very good agreement with coefficients $-\beta_1 = -0.74$, $\beta_2 = 0.53$ and $\beta_3 = 0.21$; all other components are small.

3. Comparison with numerical simulations.

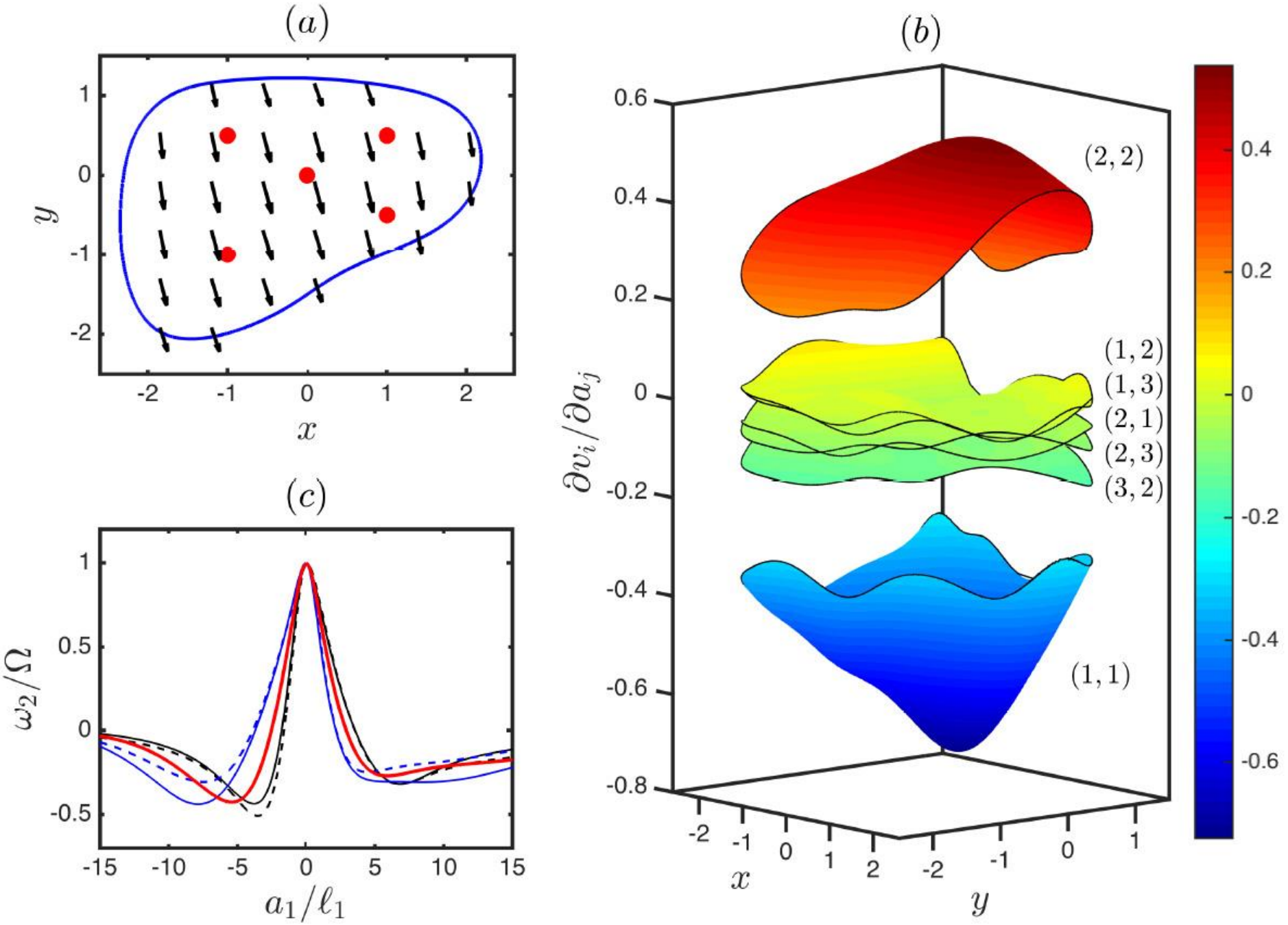

4. Simulations of different initial conditions.

We repeated our experiments for other initial conditions, starting from the shear flow,

$$\omega_x = \sin(z), \quad \omega_y = \cos(z), \quad \omega_z = 0,$$

plus periodic perturbation. We examined 3 groups of initial conditions: the 1st group – fully random periodic flow (now shear flow), the 2nd group – shear flow plus random flow in combination close to 1:1, and the 3rd group – shear flow plus small periodic perturbation. We studied 10 initial conditions for each group and used grids of up to 1024^3 total number of nodes.

We observed that

(1) all the high-vorticity regions that we checked are very well described by the exact solution, with exponential vorticity growth and pancake compression.

(2) Fully random initial conditions lead to pancakes oriented randomly in space, and this leads to final grids like 1000 x 1000 x 1000. If the shear flow is present, then the pancakes' normal directions are oriented mainly around OZ-axis, and this leads to final grids like 600 x 600 x 3000.

(3) The 2/3 scaling between the vorticity maximum and the pancake thickness is held universally,

$$\omega_{\max}(t) \sim \ell_1(t)^{-2/3}.$$

4. Simulations of different initial conditions.

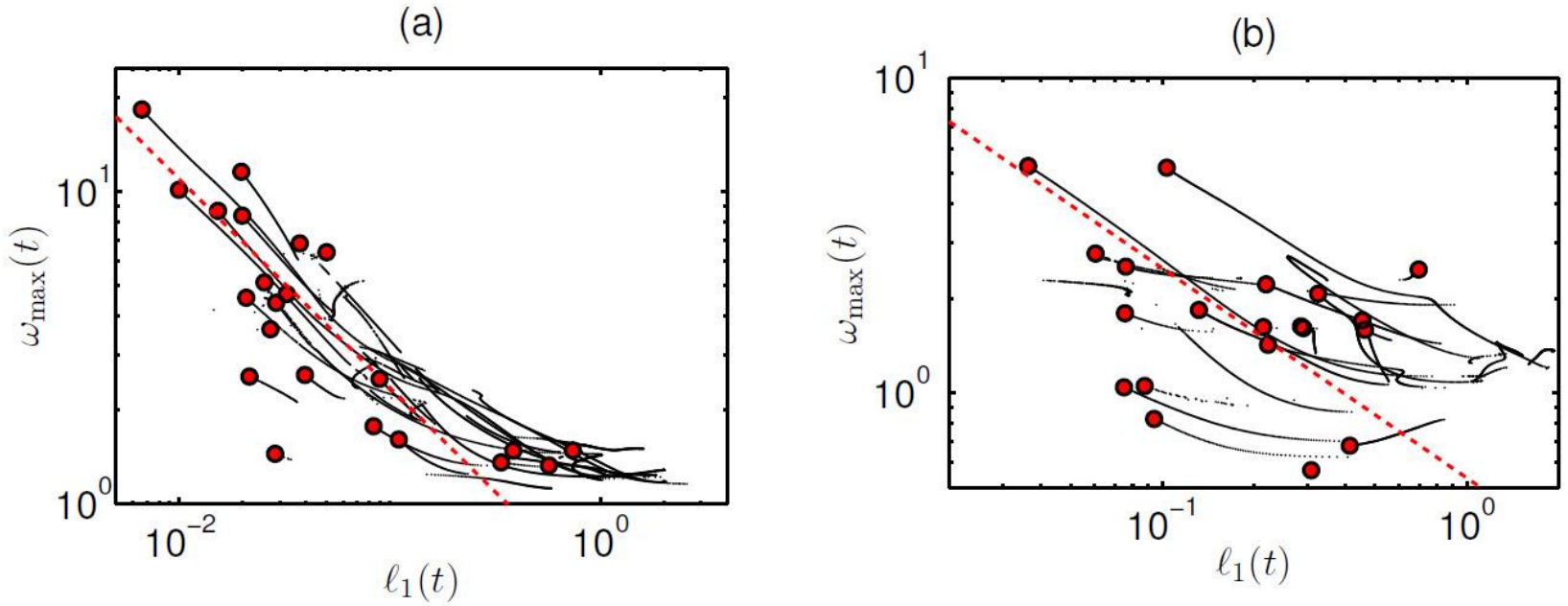

FIGURE 4. (a) Relation between the vorticity local maximums $\omega_{\max}(t)$ and the respective characteristic lengths $\ell_1(t)$ during the evolution of the pancake structures. Lines represent evolution of the maxima with increasing time, with the red dots corresponding to the final simulation time. The dashed red line indicates the power-law scaling $\omega_{\max} \propto \ell_1^{-2/3}$. (b) The same graph for a different simulation with a generic initial condition and the final grid $1152 \times 972 \times 864$.

During evolution of the pancake structures, there exists a Kolmogorov-type power-law between the vorticity maximum and the pancake thickness:

$$\omega_{\max}(t) \sim \ell_1(t)^{-2/3}.$$

4. Simulations of different initial conditions.

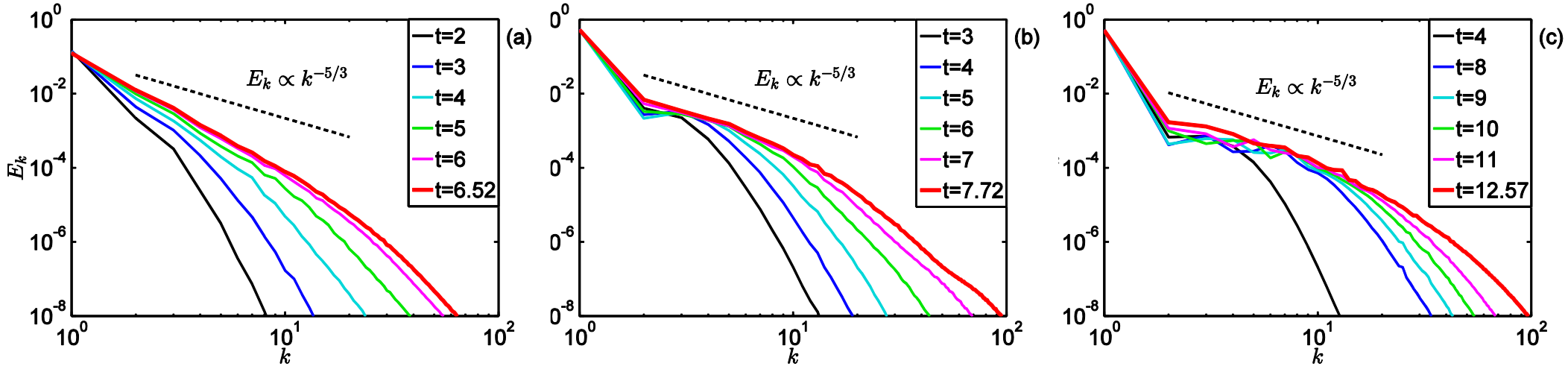

(4) The 1st group (fully random flows) does not show the Kolmogorov region $\mathbf{k^{-5/3}}$ in the energy spectrum.

5 out of 10 simulations of the 2nd group demonstrated the power-law region in the energy spectrum for wavenumbers **2 ≤ k ≤ 10**. The exponent of the power-law is close to -5/3.

Most of the 10 simulations of the 3rd group demonstrated the power-law region in the for wavenumbers **2 ≤ k ≤ 20**. The exponent of the power-law is close to -5/3.

The difference between these groups of simulations is not attributed to different final resolution (the results would be almost the same if the final resolution if z-axis would be 1000 points)!

5. Conclusions.

1. We found that the pancake-like regions of high vorticity are described asymptotically with the novel exact solution of the 3D Euler equations. The proposed solution combines a shear flow aligned with an asymmetric irrotational straining flow, and is characterized by a single asymmetry parameter and an arbitrary transversal vorticity profile.

2. A pancake structure is not completely flat with deviations much larger than the pancake thickness. It is remarkable that the proposed analytical model describes locally an every nearly flat pancake segment, while the model parameters may change from one segment to another.

3. In simulations, we observe exponential evolution of the vorticity maximum and pancake thickness, with the Kolmogorov-like relation between the two

$$\omega_{\max}(t) \sim \ell_1(t)^{-2/3}.$$

This behavior is not required by the suggested model, and presumably relates to nonlocal effects.

4. The emergence of the Kolmogorov energy spectrum can be influenced by the appropriate choice of initial conditions, which also leads to the specific orientation of the developing pancake structures. The nature this relation is yet to be discovered, and presumably is connected with the pancakes distribution.

References.

D.S. Agafontsev, E.A. Kuznetsov, A.A. Mailybaev, *Development of high vorticity structures in incompressible 3D Euler equations*, Phys. Fluids 27, 085102 (2015).

D.S. Agafontsev, E.A. Kuznetsov, A.A. Mailybaev, *Development of high vorticity in incompressible 3D Euler equations: Influence of initial conditions*, JETP Lett. 104, 685-689 (2016).

D.S. Agafontsev, E.A. Kuznetsov, A.A. Mailybaev, *Asymptotic solution for high vorticity regions in incompressible 3D Euler equations*, J. Fluid Mech. 813, R1 (2017).

Thank you for your attention!

Appendix.

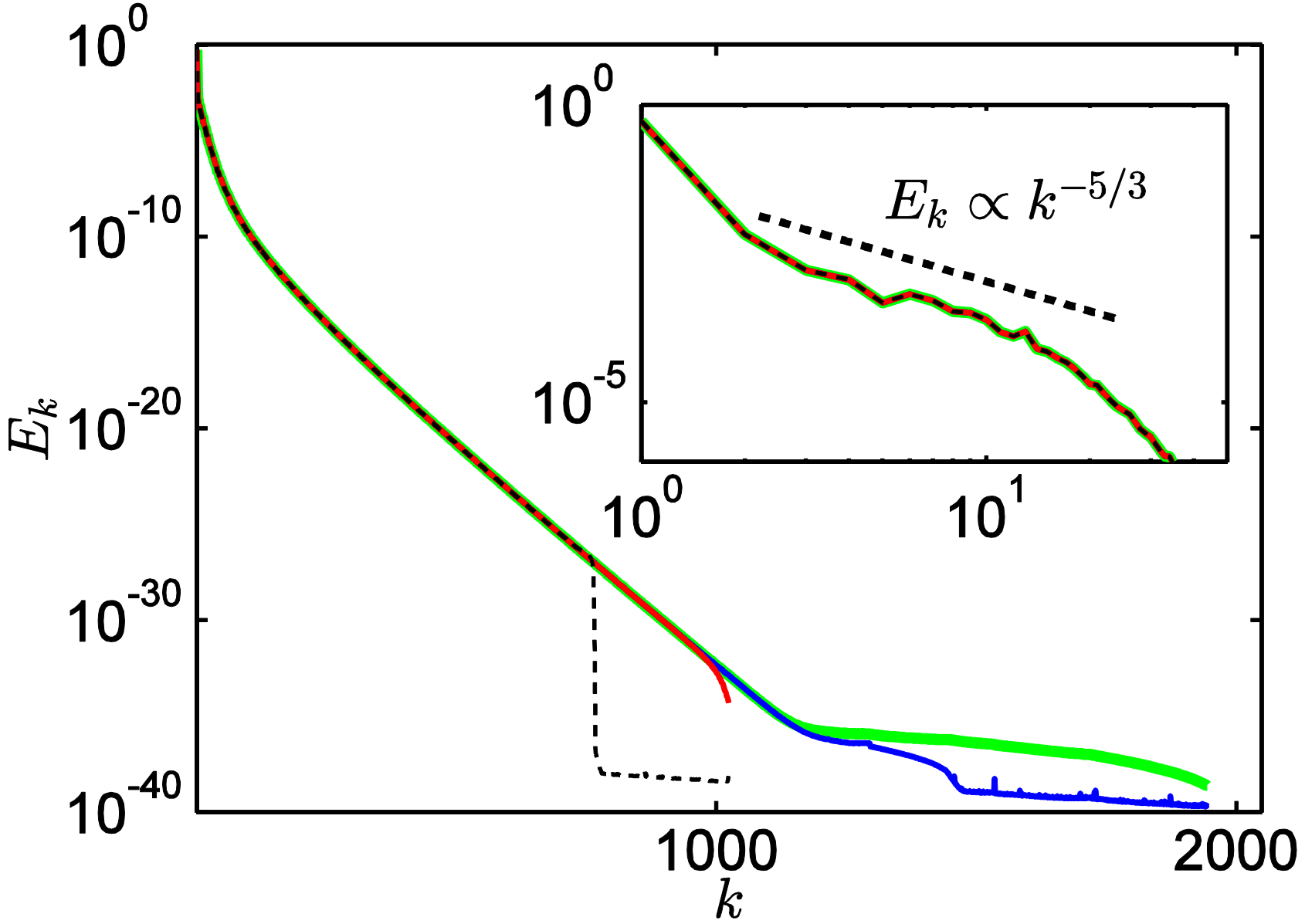
10^0
10^{-10}
10^{-20}
10^{-30}
10^{-40}
E_k
1000
2000
k
10^0
10^{-5}
10^0
10^1
$E_k \propto k^{-5/3}$